Geoderma 428 (2022) 116188

Contents lists available at ScienceDirect

Geoderma

journal homepage: www.elsevier.com/locate/geoderma

Best practice for upscaling soil organic carbon stocks in salt marshes

Cai J.T. Ladd [a,b,*], Craig Smeaton [c], Martin W. Skov [b], William E.N. Austin [c,d]

[a] School of Geographical and Earth Sciences, University of Glasgow, Glasgow G12 8QQ, UK
[b] School of Ocean Sciences, Bangor University, Menai Bridge LL59 5AB, UK
[c] School of Geography and Sustainable Development, University of St Andrews, St Andrews KY16 9AL, UK
[d] Scottish Association for Marine Science, Scottish Marine Institute, Oban PA37 1QA, UK

ARTICLE INFO

Handling Editor: Cornelia Rumpel

Keywords:
Soil organic carbon
Salt marshes
Geostatistics
Upscaling
Soil coring
Pedometric mapping

ABSTRACT

Calculating the amount of soil organic carbon (SOC) stored in coastal environments, including salt marshes, is needed to determine their role in mitigating the Climate Crisis. Several techniques exist to calculate the SOC content of a unit of land from the upscaling of soil cores. However, no comprehensive assessment has been made on the performance of commonly used SOC upscaling techniques until now. We measured the SOC content of soil cores gathered from two Scottish salt marshes. Two SOC values were used for upscaling; SOC content for a 1 m standardised depth (as recommended by the IPCC), and SOC content of the modern marsh deposit (identified in the stratigraphy as a transition from organic-rich (marsh) to mineral-rich (intertidal flat) soil. Twenty-two upscaling techniques were used (SOC content × area, interpolative, and regression-based extrapolative calculations). Leave-one-out cross-validation procedures and prediction interval widths were used to assess the accuracy of each technique. Digital Terrain Models and Normalized Difference Vegetation Indices were used as covariate surfaces in the regression models. We found that marsh-scale SOC stocks varied by as much as fifty-two times depending on which sampling depth and upscaling technique was used. The largest differences emerged when comparing SOC stocks upscaled from 1 m deep and modern marsh deposits. Using the IPCC recommended 1 m sampling depth inflated the SOC stocks of salt marshes, as intertidal flat environments were included in the calculation. Ensemble regression models from the weighted average of seven machine learning algorithm outputs produced the highest upscaling accuracies across marshes and sampling depths. Simple SOC content × area calculations produced marsh-scale SOC stocks that were comparable to stock values produced by more advanced ensemble regression models. However, regression models produced detailed maps of SOC distribution across a marsh, and the associated uncertainty in the SOC values. Our findings are broadly applicable for other environments where large-scale SOC stock assessments and uncertainty are needed.

1. Introduction

Vegetated coastlines, including seagrass, mangroves, and salt marshes, are valued for their capacity to sequester and store large amounts of organic carbon in their soils (Mcleod et al., 2011). The importance of 'blue carbon' habitats in mitigating against climate change is now widely recognised (Macreadie et al., 2019), especially given that soil organic carbon (SOC) accumulation rates in coastal habitats are expected to increase in response to sea level rise, temperature increase, and precipitation change (Rogers et al., 2019a; Wang et al. 2021; Herbert et al., 2021). However, coastal habitats are degrading globally, raising fears that blue carbon habitats could largely disappear by the end of this century (Crosby et al., 2016; Horton et al., 2018; Saintilan et al., 2022) unless significant protection and restoration efforts are enacted (Macreadie et al., 2017a; Schuerch et al., 2018). Measuring the amount of stored SOC accurately is crucial for understanding the SOC-equivalent cost of habitat loss, and for justifying financial investment in protecting and enhancing the SOC storage capacity of coastal habitats (Theuerkauf et al., 2015; Rogers et al., 2019b; Smith and Kirwan, 2021).

SOC stock assessments are based on the SOC content of soil cores. Upscaling SOC stocks from the local (soil core) to the landscape (coastal habitat) scale therefore depends on which statistical technique and soil core sampling strategy is used. Despite the publication of numerous upscaling techniques in both marine and terrestrial settings (Olaya-Abril et al., 2017; Kempen et al., 2019; Owusu et al., 2020), it remains unclear

* Corresponding author at: School of Geographical and Earth Sciences, University of Glasgow, Glasgow G12 8QQ, UK.
E-mail address: cai.ladd@glasgow.ac.uk (C.J.T. Ladd).

https://doi.org/10.1016/j.geoderma.2022.116188
Received 29 May 2022; Received in revised form 10 September 2022; Accepted 20 September 2022
Available online 25 October 2022

how different upscaling techniques affect SOC stock assessment accuracy.

Most upscaling techniques fall into one of four classes: (i) 'back-of-envelope' calculations: SOC content of single or multiple soil cores are multiplied by habitat extent; (ii) 'distance-weighted' interpolations: a prediction surface is generated between georeferenced soil core SOC values using a weighted function; (iii) 'regression' techniques: the relationship between SOC stock and predictor variables, to predict SOC stock values onto spatial covariate surfaces using machine learning algorithms, and; (iv) 'regression-kriging' techniques: an extension of regression models that also accounts for spatial autocorrelation using distance-weighted methods (Hengl and MacMillan, 2019).

Back-of-envelope calculations benefit from being relatively simple to apply (MacDonald et al., 2017) and are commonly used in large-scale, first-order assessments of SOC stocks (Atwood et al., 2017; Macreadie et al., 2017b; Rogers et al., 2019b). Distance-weighted and regression-based techniques are commonly used to produce soil carbon maps and are helpful in showing how SOC hotspots correlate with geomorphic or botanic features in the target habitat (van Ardenne et al., 2018). Regression analyses are being increasingly used over distance-weighted techniques to produce more detailed soil maps with better prediction accuracies (Li and Heap, 2011; Lieβ et al., 2016). However, the accuracy of regression models is dependent on the availability of highly correlated covariate surfaces and careful model tuning and selection (Hengl and MacMillan, 2019).

Accuracies of all upscaling techniques are improved when intensive and stratified soil core sampling is employed (Young et al., 2018). This is because variation in SOC both within and between coastal habitats can be high. Vegetation type, inundation frequency, and grain size all influence SOC accumulation rates along coastal habitats (Kelleway et al., 2016, 2017; Sousa et al., 2017; Ford et al., 2019). Microbial decomposition rates, accretion history, and site-specific physical context also influence SOC content with depth (Bai et al., 2016; Van de Broek et al., 2018). SOC content generally increases upon moving from sea to land, where more mature and organogenic deposits can become tens of metres deep (Allen, 2000; Van de Broek et al., 2018). Standard sampling of blue carbon habitats to 1 m is encouraged (Howard et al., 2014; Kennedy et al., 2014), yet not always achievable nor desirable if deposits are shallow or misrepresent much deeper deposits.

Landscape-scale SOC stock calculations can therefore differ by orders of magnitude, depending on which upscaling technique and sampling strategy is employed. For example, two national SOC stock assessments of UK salt marshes produced values which ranged between 5 (Beaumont et al., 2014) and 13 Mt SOC (Luisetti et al., 2019). Whilst back-of-envelope, distance-weighted, and regression-based extrapolation techniques have all been used to generate saltmarsh SOC inventories at global, regional, and local scales (Hinson et al., 2017; van Ardenne et al., 2018; Rogers et al., 2019a; Smeaton et al., 2022), no rigorous assessment has yet been made on the accuracy of commonly used upscaling techniques for calculating coastal habitat SOC stocks from core-based point observations.

To address this gap, we evaluate the performance of 22 commonly used upscaling techniques in generating SOC stocks for two geomorphologically distinct salt marshes along the Scottish coastline. We measured SOC content from multiple cores taken across two marshes to use as the basis of each upscaling technique.

2. Study area

Soil coring and SOC upscaling were done for Skinflats and Caerlaverock salt marshes in Scotland (Fig. 1). Skinflats is situated along the inner Firth of Forth, south-east Scotland. Skinflats is a silt-sand dominated and mesotidal marsh (Webb and Metcalfe, 1987) with a smooth profile transitioning through *Puccinellia maritima*, *Festuca rubra / Juncus gerardii*, and *Elymus repens* plant communities (Haynes, 2016). Caerlaverock marsh is situated in the hypertidal outer Solway Firth, south-west Scotland. Caerlaverock is an open-coast system, fronted by extensive tidal flats and flanked to the west by the river Nith (Marshall, 1962). Caerlaverock has a fine sand dominated substratum and a terraced topography characteristic of repeated lateral erosion and expansion phases (Allen, 1989). Abrupt shifts in vegetation community accompany the elevation changes. *Salicornia europaea* and *Spartina anglica* form the pioneer marsh, and the lower marsh is predominantly *Puccinellia maritima*. *Festuca rubra* is the dominant species at the high marsh, which extends into the transitional marsh zone alongside *Juncus effusus*, *Carex flacca*, and *Leontodon autumnalis* (Haynes, 2016). Cattle grazing along fenced parts of the upper marsh maintain a short sward height. Skinflats is relatively narrow (250 m) and small (60 ha), compared to Caerlaverock which ranges in width by between 1 and 1.5 km, and has a contiguous extent of ~ 920 ha.

3. Methods

Soil cores were used to calculate the SOC content of Skinflats and Caerlaverock salt marshes. Two values of SOC content per core were calculated (SOC content of the full core, and SOC content of the modern marsh deposit only, see section 3.1). Both SOC calculations were then used to generate separate marsh-scale SOC stocks using twenty-two upscaling techniques divided into four classes of statistical analysis type (see section 3.2). Uncertainty in each calculation was also calculated (see section 3.3). A total of 88 stock assessments were produced (2 marshes × 2 soil core SOC values × 22 upscaling techniques) (Fig. 2). The stock calculations produced here represent a snapshot of the SOC present in each marsh from the time of sampling. The stocks therefore do not account for changes in the long-term storage of SOC affected by processes including microbial decomposition, autochthonous production, and mineralisation of labile organic matter. All analyses were carried out using R, and the code is available in Appendix A.

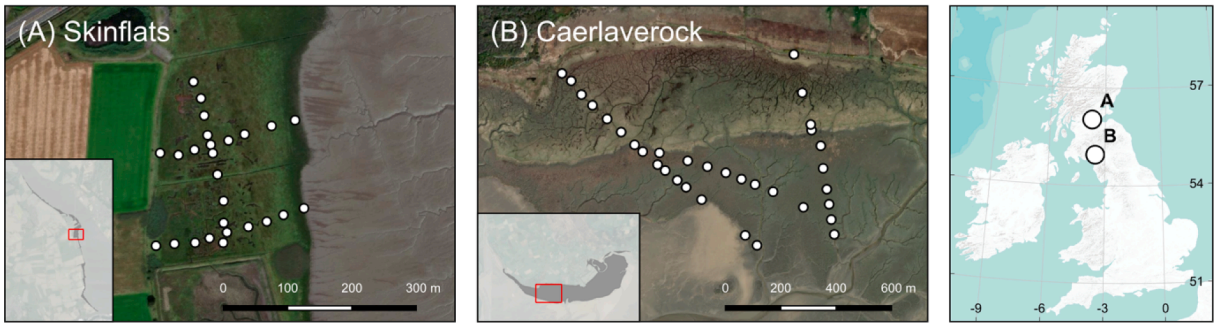

Fig. 1. **A** Skinflats (56°03′33″N, 003°44′05″W) and **B** Caerlaverock (54°58′07″N, 003°30′39″W) salt marshes, Scotland. White points indicate soil core sampling locations.

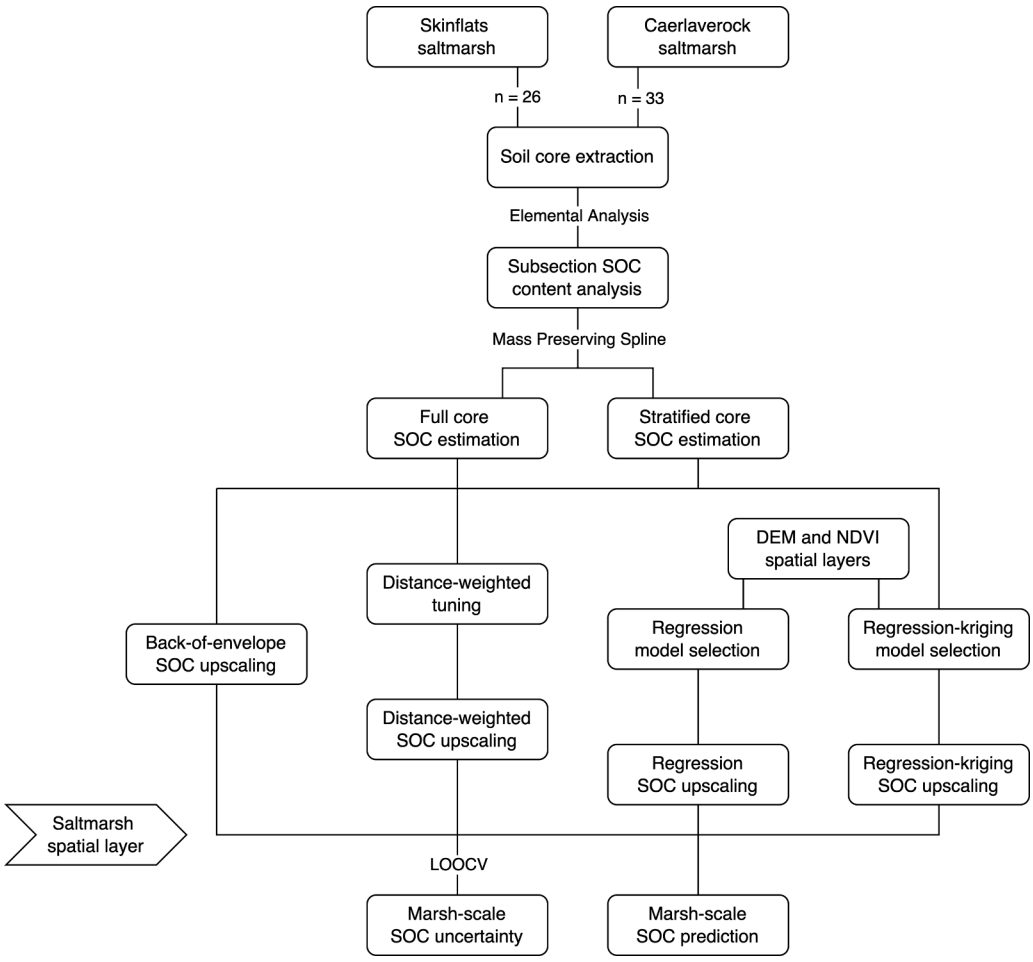

Fig. 2. Steps taken to generate marsh-scale soil organic carbon stock calculations.

3.1. *Quantifying the organic carbon content of soil cores*

Soil cores were taken from Skinflats and Caerlaverock in the summer of 2019. Cores were retrieved along three transects at each site. Two transects were placed perpendicular to the shore intersecting high- to low-marsh zones, and a third transect ran diagonally on the shore intersecting the two other transects (Fig. 1; white points). Sampling interval was adjusted to capture any abrupt change in vegetation composition and elevation. Coordinates of each coring site were taken using a real-time-kinematic GPS to an average accuracy of ~ 2 cm. Soil coring was done using a narrow (30 mm) Eijkelkamp gouge auger. Gouge coring has been shown to cause minimal compaction of the sampled soil (Smeaton et al., 2020). To extract soil cores, the gouge auger was pushed by hand into the ground to either a depth of 1 m or until a resistant basal layer was reached. Properties of the soil core were then described using the Tröels-Smith classification scheme (Tröels-Smith, 1955) to provide a stratigraphic definition of where the modern saltmarsh deposit begins, typically defined as a basal transition from organic-rich to organic-poor, mineral soils (Hamilton et al., 2015; Swindles et al., 2018; Smeaton et al., 2020). Cores were then sub-sectioned in the field at depths of 0–2, 4–6, 10–12, 20–22, 30–32 and so on, until 90–92 cm. In total, 26 cores were recovered from Skinflats and 33 from Caerlaverock.

Each 2 cm soil sample was dried (50 °C, 48 h) and weighted to calculate dry bulk density. No rock fragments were found in the soil samples, and so did not affect bulk density measurements. We only considered the presence of organic soil carbon deposits in this study, and therefore excluded any carbon contribution from calcareous (inorganic) material. The dried soil was milled and homogenised, and a 10 mg sub-sample was placed in a silver capsule and treated with HCl through acid fumigation to remove carbonates (Harris et al., 2001). After further drying (50 °C, 24 h), the samples were analysed for SOC content using an Elementar EL Vario (Verardo et al., 1990; Nieuwenhuize et al., 1994). Analytical precision of SOC content was estimated from repeat analyses of standard reference material B2178 (Medium Organic Content Standard; Elemental Microanalysis, UK). Standards deviated from known SOC reference values by 0.09 % (n = 38). Total organic carbon and dry bulk density values for cores from each marsh are shown in Fig. S1-4.

A mass preserving spline (Bishop et al., 1999) was used to produce continuous SOC density values along the length of each soil core (Fig. S5-6; black line). Two values of SOC stock per core were calculated. The first SOC stock represented the sum of 1 cm SOC density subsection values across the entire core, following the recommended method outlined by Howard et al. (2014) and by the Intergovernmental Panel on Climate Change (IPCC) (Kennedy et al., 2014) for implementing national greenhouse gas inventories. These SOC stock values are henceforth referred to as 'full core' SOC stock values. As retrieving 1 m cores was not possible in all cases, 'full core' SOC stocks were standardised by core length to account for different coring depths between samples. The second SOC stock represented the sum of 1 cm SOC density subsection values to the bottom of modern marsh deposits (i.e., to the red dotted lines of each core in Fig. S5-6), representing SOC content of the saltmarsh habitat only. These SOC stock values are henceforth referred to as 'stratified core' stocks.

3.2. Measuring the carbon stocks of saltmarshes from soil cores

Marsh-scale SOC stocks were calculated from the SOC content of soil cores, using 22 upscaling techniques frequently used for generating SOC stock assessments (Table 1). The areal extent of each salt marsh was used as a template upon which SOC values were mapped. Saltmarsh extents were taken from Haynes (2016). The geospatial vector data was converted to a raster format in a geographic information system, to produce maps showing SOC stocks at a standard resolution of 2 m^2 (chosen as the smallest possible resolution, see section 3.2.1). The sum of raster cell values multiplied by the area of the cell were used to calculate the total SOC content per upscaling technique.

All 22 upscaling techniques can be divided into 4 classes of SOC calculation (Table 1). The 'back-of-envelope' class assign SOC values to a raster cell based on the SOC content of single or multiple soil cores. The 'distance-weighted' class assign SOC values as a function of distance between points, weighted by the SOC content of surrounding points (Hengl and MacMillan, 2019). The 'regression' class use the relationship between response (SOC values) and predictor variables (see section 3.2.1) to build a regression model. The model coefficients are then used to predict SOC values of each covariate raster cell (Li et al., 2011). Lastly, the 'regression-kriging' class attempts to improve the 'regression' class predictions by accounting for any spatial autocorrelation between points. This is done by adding the predictions generated by regression with ordinary kriging of the residuals (Knotters et al., 1995). In both 'regression' and 'regression-kriging' classes, an additional marsh-scale SOC surface calculation, called 'ensemble', was generated by averaging the SOC value per raster cell across all regression or regression-kriging calculations. Averaging was weighted against the R^2 score between observed and predicted values (see section 3.3) of each regression or regression-kriging model (Hengl and MacMillan, 2019). The 'gstat' package was used to fit the Inverse Distance Weighting model (Pebesma, 2004) and the optimal power decay rate was selected through model tuning (see Appendix A). The 'automap' package was used to determine the optimum variogram model of the residuals necessary to quantify autocorrelation in the ordinary kriging and all regression-kriging techniques (Hiemstra, 2013). All semivariogram models are reported in Appendix A. The 'caret' package was used for model tuning and for fitting each optimal regression model (Kuhn, 2008). Parameters selected from the model tuning through a cross-validation procedure for each regression model are shown in Appendix A.

3.2.1. Selecting predictor variables for regression-based upscaling

All regression-based upscaling techniques used a set of predictor variables when calculating SOC values. When considering which predictor variables to use in our study, we referred to Jenny (1994) who describe soil SOC stock as a function of soil composition, climate, vegetation, relief, geology, and time. Continuous spatial layers of covariates can predict SOC stock for a given area when the correlation between the predictor variable and the response variable is high (Hengl and MacMillan, 2019). We excluded climate and underlying geology as predictor variables of SOC stock since the variability of both at the marsh-scale would likely be negligible. Although national layers of soil (including moisture content, grain size and soil texture) and vegetation (National Vegetation Classification surveys) composition exist for Scotland (e.g., Haynes, 2016; LandIS, 2020), these were considered too coarse or had inconsistent coverage to use in the upscaling procedure. Spectral reflectance of vegetation was instead used to detect variation in vegetation health, identity, and underlying soil composition. The Normalised Difference Vegetation Index (NDVI) is a commonly applied plant-soil index and was used here as a proxy for distinguishing vegetation and soil texture types (Gholizadeh et al., 2018).

Continuous NDVI spatial layers for Skinflats and Caerlaverock were generated from remote sensing. Cloud-free Sentinel-2 images from 04 to 07-2019 and 27–06-2019 were downloaded from the Copernicus Open Access Hub (2021). The images had undergone Level-2A processing,

Table 1
Description of the 22 upscaling techniques, divided into 4 classes, used to create SOC maps for Skinflats and Caerlaverock salt marshes. See Appendix A for a full description of the analysis.

Class and technique	Code	Calculation of soil organic carbon value per raster cell
Back-of-envelope		
High	HIGH	SOC value of a single soil core taken from the high marsh zone.
Mid	MID	SOC value of a single soil core taken from the mid marsh zone.
Average (transect)	TRAN	Average SOC value of multiple soil cores taken along a land-to-sea transect.
Average (all)	ALL	Average SOC value of all soil cores.
Distance-weighted		
Inverse distance weighting	IDW	SOC values around each core location are interpolated from the weighted average value of nearby points and the inverse of the distance between those points as a power decay function.
Ordinary kriging	OK	Similar to IDW, however spatial autocorrelation was used as a weighting function rather than distance.
*Regression and regression-kriging**		
Generalised linear model	GLM	Coefficients of the regression model used to calculate the SOC values of each raster cell. Weighted sum of the SOC predictor variables input into the linear model using a Gaussian link function.
Generalised additive model	GAM	Coefficients of the regression model used to calculate the SOC values of each raster cell. Weighted sum of the SOC predictor variable input into the model using spline functions (calculated automatically using a restricted maximum likelihood model) that best represented non-linear trends.
Random forest	RF	Coefficients of the regression model used to calculate the SOC values of each raster cell. Regression trees and branches grown from a bootstrap sample of the SOC predictor variables.
Bayesian regularised neural network	BRNN	Coefficients of the regression model used to calculate the SOC values of each raster cell. An optimal model found from building successive mathematical structures between SOC value and SOC predictor variables from weighted values of preceding models.
Cubist	CUB	Coefficients of the regression model used to calculate the SOC values of each raster cell. The model is identified by partitioning SOC values amongst groups of correlated SOC predictor variables using a hierarchical set of rules that follow an "if [condition is true] then [regress] or else [apply the next rule]" statement.
Stochastic gradient boosting	SGB	Coefficients of the regression model to calculate the SOC values of each raster cell. A combination of bagging and boosting approaches is used for model selection.
Support vector machine	SVM	Coefficients of the regression model to calculate the SOC values of each raster cell. A model is constructed from kernel functions that re-projected SOC predictor values as vectors onto a hyperspace to identify non-linear patterns in SOC.
Ensemble	ENS	Average of all 7 regression model predictions, weighted by the R^2 score between observed and predicted SOC values of each prediction.

*Regression-kriging combines the output of the regression models with ordinary kriging of the regression residuals, to account for possible error introduced by spatial autocorrelation. Regression models have the suffix '.R', whilst regression-kriging models have the suffix '.RK'.

meaning that images were geometrically, radiometrically and atmospherically corrected (Mayer and Kylling, 2005). NDVI was calculated by:

$$NDVI = \frac{(B_8 - B_4)}{(B_8 + B_4)}$$

Where B_4 and B_8 represent the red (650–680 nm) and near infrared (785–899 nm) Sentinel-2 spectral bands respectively. The resolution of the final NDVI layer was 10 m.

Saltmarsh elevation is a good proxy of soil age, vegetation structure, and soil composition in marshes (Allen, 2000). Digital Terrain Models (DTMs) are available for much of Scotland and were therefore also used as a predictor of SOC stock for both marshes. DTMs with 2 m resolution, retrieved using Light Detection and Ranging aerial surveys, were downloaded from EDINA Digimap (2019) for Skinflats and Caerlaverock (2016–11-14). The Skinflats DTM was cropped to remove cells relating to bridge construction works above the marsh. NDVI and DTM surfaces for both marshes were resampled into spatial rasters with a 2 m^2 cell size and cropped to fully overlap one another. The location of each soil core was then overlaid onto the covariate rasters, and the cell value from each raster was extracted and used as the predictor variables in the regression models.

Distributions, outliers, and collinearity between predictor variables for SOC, NDVI, and DTM values were then inspected. Response and predictor variables were all normally distributed. Soil cores 8 and 26 in Skinflats reported NDVI and DTM values that were substantially below the mean and standard deviation values of the sample population (see Appendix A). Both soil core samples were taken at the salt marsh-tidal flat interface. It is possible that NDVI and DTM values did not accurately represent the marsh where the cores were taken. The coarse (10 m) resolution of Sentinel-2 images likely included reflectance from the tidal flat within the cell value, resulting in a lower NDVI index than expected for the vegetated marsh where the cores were taken. The marsh also appeared to have expanded seaward since LiDAR data was collected in November 2016, meaning that the DTM values represented lower-elevation tidal flats as opposed to the higher-elevation marshes where the soil cores were taken. For these reasons, soil cores 8 and 26 were identified as outliers and excluded from the regression analyses.

Correlation plots between predictor variables showed no evidence of collinearity for either marsh. Selection of predictor variables to use in the regression analyses was done by inspecting correlation plots for relationships with the response variables (linear or otherwise) and confirmed by inspecting the Akaike Information Criterion in a stepwise linear regression with forwards and backwards model selection. For Skinflats, DTM and NDVI showed no significant relationship with the full and stratified SOC values respectively, and were dropped from further analysis. For Caerlaverock, NDVI showed no significant relationship with either the full or stratified cores. NDVI observations for Caerlaverock were therefore dropped.

3.3. Assessing the uncertainty of carbon stock values

Uncertainty of each upscaling technique result was assessed using a leave-one-out cross-validation (LOOCV) resampling procedure. LOOCV leaves out one sample when generating a SOC map, then predicts the SOC value of that removed point based on its location on the map. This is repeated until all samples have been left out once. Two datasets are produced using LOOCV: predicted SOC values for each point observation, and a series of marsh-scale SOC maps each generated from all-bar-one of the points. The predicted values were then correlated against their corresponding observed values to generate an R^2 statistic, root mean square error (RMSE), and mean absolute error (MAE) of predicted SOC values. The correlation plots of observed and predicted values were then checked for evidence of model bias (i.e., the overestimation or underestimation of predictions) and non-constant variance (i.e., whether the full range of SOC values were represented). Uncertainty maps were produced by extracting the 90 % prediction interval width (i.e., the difference between the 5 % and 95 % quantiles) for each raster cell of overlapping maps produced by the LOOCV procedure. These 'uncertainty maps' were used to assess the performance of each SOC upscaling technique. A lower resolution raster size of 10 m^2 was used to generate the uncertainty maps to reduce computing time. No uncertainty assessment could be made for 'HIGH' and 'MID' upscaling techniques since these are based on single cores only. For 'TRAN' and 'ALL' techniques, LOOCV would result in R^2 values with a perfect fit (i.e., $R^2 = 1$) since the observed and predicted points for each LOOCV iteration would be the same. Given that the R^2 value would not give a meaningful indication of uncertainty in these cases, they were not reported in the results.

4. Results

4.1. Uncertainty assessment

Uncertainty metrics for each upscaling technique and observed-predicted relationships of the best-performing techniques in each class (i.e., techniques that yielded the lowest RMSE score) are shown in Table 2 and Fig. 3 respectively. Of the best performing 'back-of-envelope' class, mean SOC values derived from shore-normal transects yielded the lowest RMSE and MAE values across both marshes and sampling depths (Table 2). However, bias (i.e., the over- and under-prediction of SOC values away from the dashed 1:1 line) was high (Fig. 3 A, E, I, M). For the best performing 'distance-weighted' models, R^2 values were comparable (R^2 = 0.33–0.52) except for Caerlaverock (stratified cores) that yielded a lower R^2 value of 0.12 (Table 2). Of these, only Caerlaverock (full cores) showed low bias (Fig. 3 B, F, J, N). Regression-kriging ensemble techniques consistently reported the lowest uncertainty scores across all mashes and depths (Table 2). R^2 values for Caerlaverock were higher (0.48–0.61) than Skinflats (0.00–0.26) for all singular regression and regression-kriging class models when full cores were used to calculate SOC stock. Values were comparable and low (0.00–0.29) when stratified cores were used (Table 2). When models were combined as ensembles, however, R^2 values were comparable and high for regression and regression-kriging techniques (0.59–1.00) across both sampling depths (Table 2). The ensemble models generally showed low bias (Fig. 3 C-D, G-H, K-L), except for Caerlaverock (stratified cores) that tended to underpredict SOC values (Fig. 3 O—P). Regression model performance only marginally improved with kriging, likely due to little evidence of spatial autocorrelation amongst the soil core samples (see Appendix A).

4.2. Marsh-scale carbon stocks and uncertainties

Spatial calculations of marsh-scale SOC stock and corresponding prediction interval widths (a measure of model uncertainty) for the best performing models (see Table 2) are shown in Figs. 4-7. Surfaces derived from TRAN calculations showed a homogeneous coverage of SOC and prediction interval widths across each marsh (Figs. 4-7 A-B). Distance-weighted surfaces also homogenised ~ 50 m away from where the soil cores were taken (Figs. 4-5 and 7 C), apart from Caerlaverock (full core) where the OK model showed a general decrease in SOC stock moving from the landward to seaward edge (Fig. 6 C). Prediction interval width values increased along the same gradient (Fig. 6 D). ENS.R (Figs. 4-7 E) and ENS.RK (Figs. 4-7 G) models produced similar SOC calculations across each marsh and sampling depth. The ensemble regression-based surfaces captured more abrupt changes in SOC than back-of-envelope and distance-weighted classes. For Caerlaverock, SOC values declined abruptly beyond a marsh cliff (Fig. S7) by ~ 30 % for both sampling depths (Figs. 6-7 E-G), characterised as a drop in elevation and change in vegetation community. For the ENS models, elevated SOC values were calculated near the seaward marsh edge and channels for Skinflats (Figs. 4-5 E-G) and at a feature in the north-east corner of Caerlaverock

Table 2
R^2, Root Mean Squared Error (RMSE) and Mean Absolute Error (MAE) terms for 22 upscaling techniques. Best performing models from each model class are shown in bold. No RMSE, MAE, and R^2 values are reported for 'HIGH' and 'MID' techniques since these used only a single value of SOC. R^2 is not reported for 'TRAN' and 'ALL' since predicted values produced perfect fits.

	Skinflats						Caerlaverock					
	Full core			Stratified core			Full core			Stratified core		
Class and technique	R^2	RMSE	MAE	R^2	RMSE	MAE	R^2	RMSE	MAE	R^2	RMSE	MAE
Back-of-envelope												
HIGH	–	166.72	136.46	–	22.61	19.36	–	140.64	127.30	–	19.45	10.88
MID	–	245.69	210.49	–	23.24	17.77	–	109.77	95.06	–	19.53	10.86
TRAN	–	**115.74**	**92.02**	–	**14.83**	**13.22**	–	**101.71**	**88.23**	–	**19.01**	**13.70**
ALL	–	140.61	114.42	–	17.01	13.48	–	103.13	83.65	–	19.36	12.68
Distance-weighted												
IDW	**0.33**	**115.79**	**99.22**	0.08	17.45	14.15	0.36	85.39	59.52	**0.12**	**17.75**	**10.02**
OK	0.13	126.56	105.47	**0.41**	**17.66**	**14.12**	**0.52**	**69.65**	**52.76**	0.12	17.81	10.40
Regression												
GLM.R	0.07	133.87	99.66	0.00	17.15	13.33	0.57	66.13	50.83	0.16	17.52	11.91
GAM.R	0.22	123.74	95.29	0.29	13.80	10.84	0.57	66.13	50.83	0.16	17.52	11.91
RF.R	0.17	127.03	96.83	0.12	15.44	13.02	0.50	72.70	55.30	0.09	20.10	13.42
BRNN.R	0.06	145.60	116.01	0.02	18.69	14.94	0.51	72.61	53.61	0.15	17.57	11.90
CUB.R	0.14	129.82	94.87	0.03	16.82	14.05	0.58	65.70	50.49	0.20	17.20	11.32
SGB.R	0.16	126.38	98.14	0.20	14.40	12.12	0.54	67.93	50.75	0.10	17.94	12.00
SVM.R	0.13	130.38	93.51	0.01	16.74	12.79	0.61	64.57	47.53	0.20	17.77	10.26
ENS.R	**0.59**	**96.95**	**69.91**	**0.80**	**8.54**	**6.75**	**0.70**	**55.53**	**42.27**	**0.37**	**15.12**	**9.85**
Regression-kriging												
GLM.RK	0.20	123.52	95.05	0.01	17.57	13.61	0.58	65.21	48.83	0.16	17.58	11.84
GAM.RK	0.26	120.89	95.97	0.16	15.64	11.86	0.57	65.47	49.11	0.16	17.59	11.83
RF.RK	0.22	123.89	95.16	0.04	16.87	13.98	0.48	74.89	56.58	0.08	20.44	13.62
BRNN.RK	0.00	140.44	116.53	0.02	17.22	13.16	0.56	66.55	50.94	0.16	17.59	11.84
CUB.RK	0.22	123.28	90.47	0.01	17.48	14.54	0.59	64.74	50.17	0.19	17.36	11.60
SGB.RK	0.23	121.04	96.05	0.13	15.17	12.52	0.53	68.38	51.79	0.08	18.48	12.34
SVM.RK	0.20	123.43	94.44	0.00	16.87	13.07	0.60	63.84	47.16	0.14	17.46	11.37
ENS.RK	**0.95**	**50.93**	**36.31**	**0.92**	**6.44**	**5.12**	**1.00**	**5.46**	**4.24**	**0.79**	**10.49**	**6.91**

(Figs. 6-7 E-G) that greatly exceeded the SOC stock values obtained from the soil cores (see x-axis on Fig. 3). Prediction interval width values at these locations were also highest (Figs. 4-7, F-H), indicating these SOC values are unreliable and the result of extrapolation beyond the range predictor (DTM and NDVI surfaces) and response (observed soil core SOC) values used to fit the regression models.

4.3. Carbon budget assessment

Values of the total SOC content for each marsh section (i.e., the extent represented in Figs. 4-7), calculated from full and stratified soil cores for 22 upscaling techniques, are shown in Fig. 8. For Skinflats and Caerlaverock, the greatest difference in SOC values when comparing across all techniques and sampling depths were 52 and 24 times respectively. When averaged across all upscaling techniques, total SOC values for Skinflats and Caerlaverock were 16 and 10 times lower respectively when stratified soil cores were used over full cores. For each marsh and sampling depth, SOC values ranged by 41–55 % between upscaling techniques, except for Skinflats (stratified) where values ranged by as much as 86 %. Back-of-envelope calculations (HIGH, MID, TRAN, and ALL) ranged by 27–54 % across both marshes and sampling depths. HIGH calculated more SOC content than MID in all cases, although the range difference was much lower (3 %) for Caerlaverock (stratified) than the other techniques (that ranged by 17–54 %). ALL produced higher values of SOC than TRAN for Skinflats, and the pattern was reversed for Caerlaverock. The range difference was only 5–24 %. There was no consistent trend in whether TRAN and ALL calculations were higher or lower than HIGH and MID (Fig. 8).

Distance-weighted classes (IDW and OK) calculated total SOC values that differed by 2–19 % for Skinflats and Caerlaverock. For Caerlaverock, prediction interval widths (error bars) were markedly higher than IDW when stratified cores were used. SOC values from distance-weighted classes were comparable to TRAN and ALL values. Regression and regression-kriging model calculations were comparable within all marshes and sampling depths. The largest difference was found in Caerlaverock (stratified), where the SVM.R and SVM.RK values differed by 33 %. For SOC values derived from full depth cores, regression-based calculations ranged by 14–18 %. In contrast, calculations ranged by 86 % for Skinflats and 43 % for Caerlaverock when stratified cores were used. The range difference was driven by high GAM calculations for Skinflats (stratified) and low SVM.R calculations for Caerlaverock (stratified). Because GAM regressions yielded the highest R^2 values compared to all other regression-based models for Skinflats (stratified), ENS calculations (i.e., the calculation weighed by the R^2 performance of each regression model) fell in between the GAM and other regression calculations. The high R^2 scores from the GAM regression was likely caused by overfitting from poorly correlating variables (see Appendix A).

5. Discussion

Our study demonstrates that marsh-scale SOC stock calculations can differ by as much as 52 times depending on how upscaling from the scale of 'soil core' to 'salt marsh' is done. The reliability of SOC upscaling depends upon (i) which technique is used, (ii) how well covariates predict SOC stock (if a regression-based method is used), and (iii) whether soil core SOC values from a standardised depth (e.g., 1 m according to IPCC standards) or stratified depth (e.g., only marsh deposits whilst excluding deeper stratigraphic horizons equivalent to tidal flat or glacial environments) are used. Differences in the approach taken when calculating habitat-scale SOC stocks would have significant consequences on ecosystem service valuations. For example, the value of carbon credits in 2010 for regulated markets was estimated at $19.18 USD/Mg (Ullman et al., 2013). Since Skinflats and Caerlaverock marshes

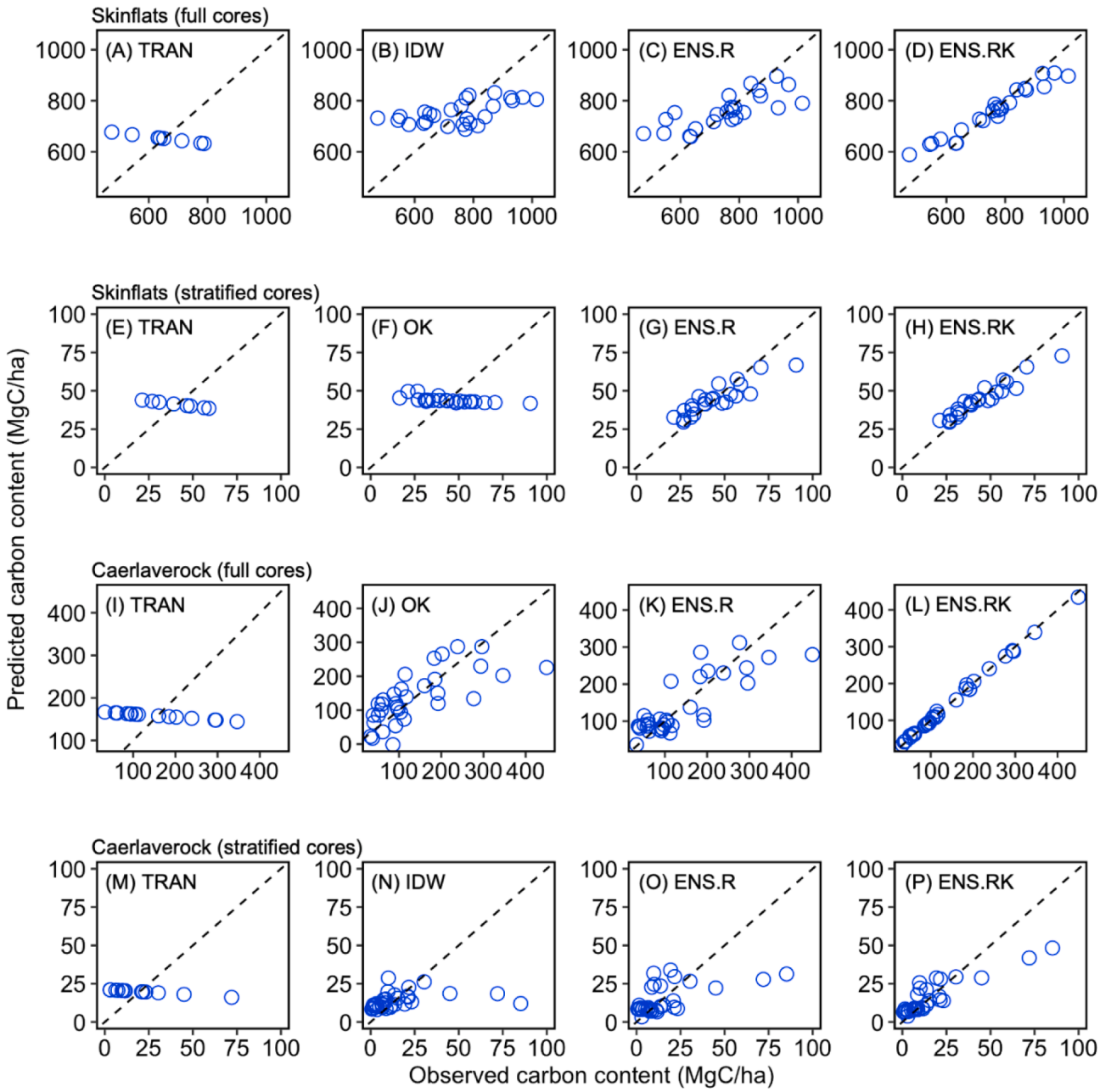

Fig. 3. Correlations between observed and predicted SOC stock values for the best performing upscaling techniques of each class (see Table 2) for Skinflats and Caerlaverock marshes using SOC values from full or stratified cores. Predicted values are derived from a leave-one-out cross validation resampling procedure. Dashed line indicates a perfect fit of observed and predicted values. See Appendix A for all observed-predicted relationships.

had SOC stocks that ranged by as much as 21,000 and 77,000 MgC respectively, valuations would range by $400,000 and $1,500,000 USD per site. These values do not take inflation and gain in the value of SOC into account since 2010, and only represent the section of each marsh considered here - not the full extent. Differences in valuation would therefore be expected to be even higher. Blue carbon stock assessments are being increasingly used to underpin social and ecological sustainability programmes including habitat conservation and restoration projects (Gulliver et al., 2020), payments for ecosystem services schemes (Thompson et al., 2017), and climate change mitigation and adaptation policies (Hilmi et al., 2021). It is therefore imperative that an appropriate upscaling technique is used when calculating SOC stocks.

The largest differences in SOC stock calculations arose when SOC values from either standardised 1 m cores or from modern marsh deposits alone were used. IPCC guidelines (Kennedy et al., 2014) and the Blue Carbon Manual (Howard et al., 2014) recommends that a standard sampling depth of 1 m should be used when assessing the SOC stocks of coastal ecosystems. Whilst a standardised depth of sampling makes it easier to compare between ecosystems (Duarte et al., 2013), marsh deposits in this study were shallow. Deposits only reached a maximum of 16 and 22 cm for Skinflats and Caerlaverock respectively, resulting in near-surface marsh-scale SOC stocks that were as much as 16 times lower than if 1-metre standardised cores were used for upscaling. Sediment SOC stores beneath modern marsh deposits may represent paleo-habitats, such as intertidal flats before marsh colonisation, or terrestrial soils flooded during sea level transgression (Shi and Lamb, 1991). Including such 'pre-marsh' deposits in stock calculations risks inflating the actual SOC storage value of modern salt marsh deposits. Habitat-specific blue carbon stocks are frequently cited when extoling ecosystem service benefits (e.g., Duarte et al., 2013) and are used in

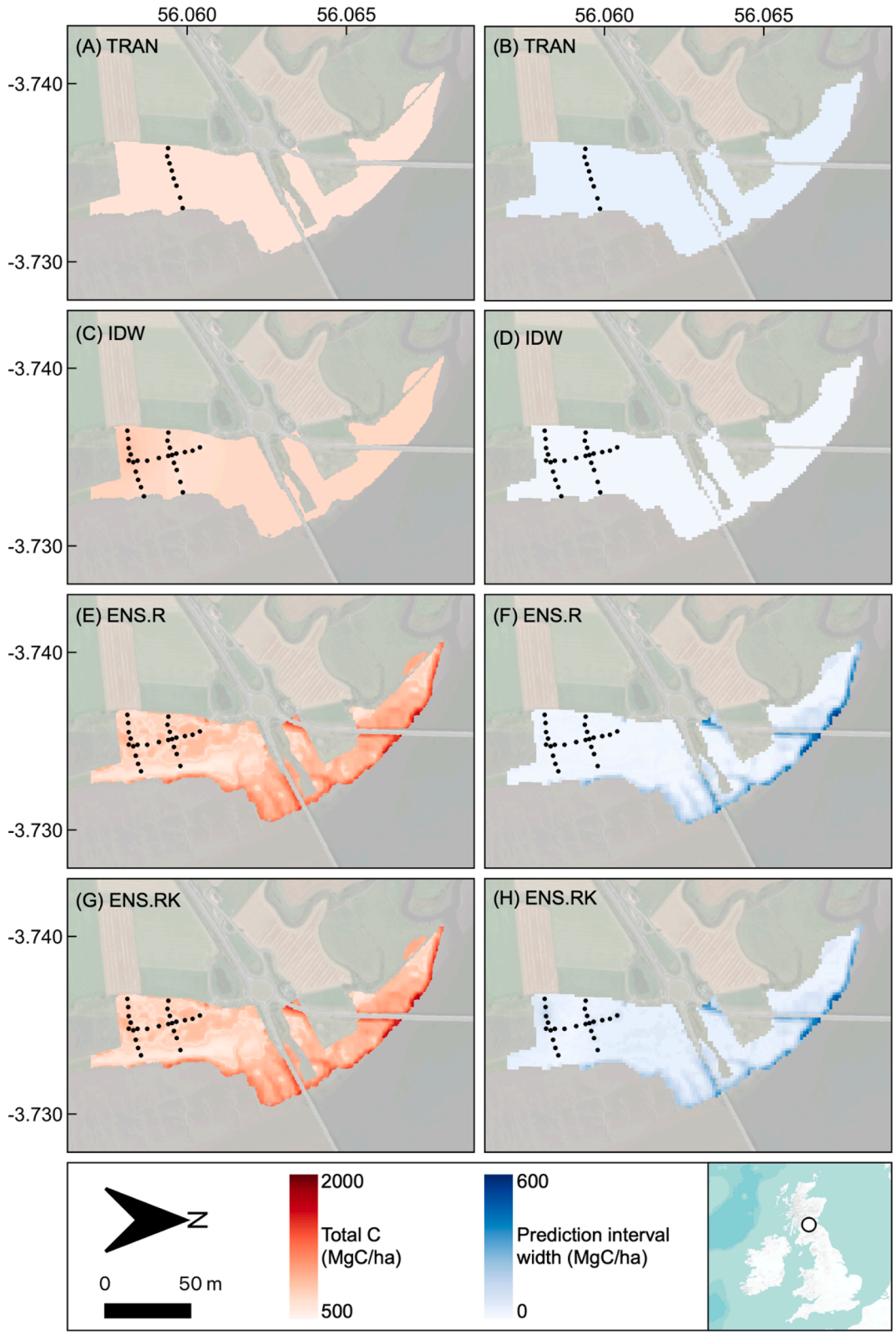

Fig. 4. Stock (red) and uncertainty (blue) of SOC upscaled from full soil cores for a section of Skinflats salt marsh, Scotland. Each map was generated from the best performing technique for each upscaling class (see Table 2). The specific upscaling technique is reported in each map panel. Uncertainty is presented using the 90% prediction interval width calculated from a leave-one-out cross validation resampling procedure, where high values indicate greater uncertainty. Normalised Vegetation Difference Index was used as the predictor in the regression models. Black dots indicate the location soil cores were gathered. (For interpretation of the references to colour in this figure legend, the reader is referred to the web version of this article.)

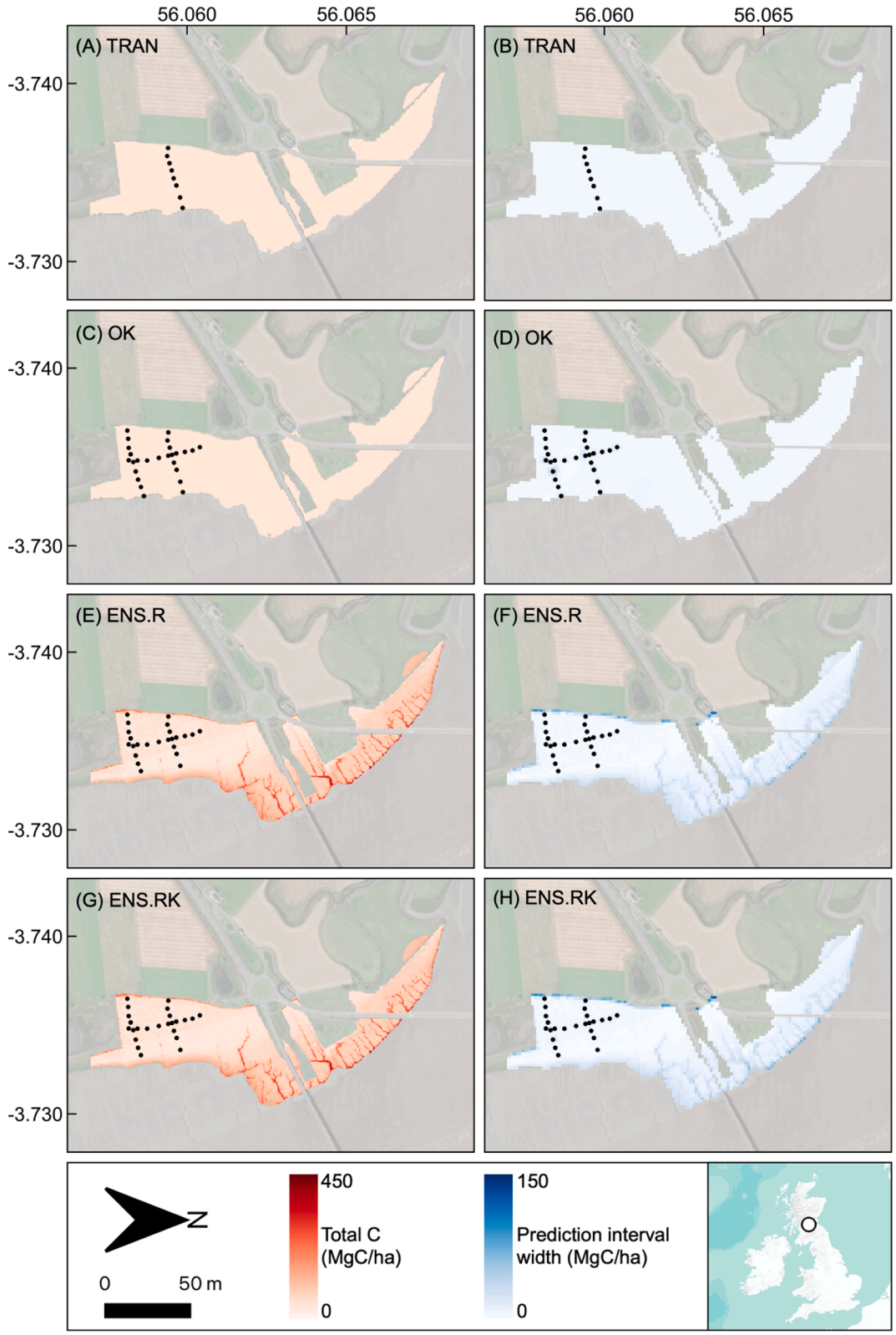

Fig. 5. Stock (red) and uncertainty (blue) of SOC upscaled from stratified soil cores for a section of Skinflats salt marsh, Scotland. Each map was generated from the best performing technique for each upscaling class (see Table 2). The specific upscaling technique is reported in each map panel. Uncertainty is presented using the 90% prediction interval width calculated from a leave-one-out cross validation resampling procedure, where high values indicate greater uncertainty. Elevation was used as the predictor in the regression models. Black dots indicate the location soil cores were gathered. (For interpretation of the references to colour in this figure legend, the reader is referred to the web version of this article.)

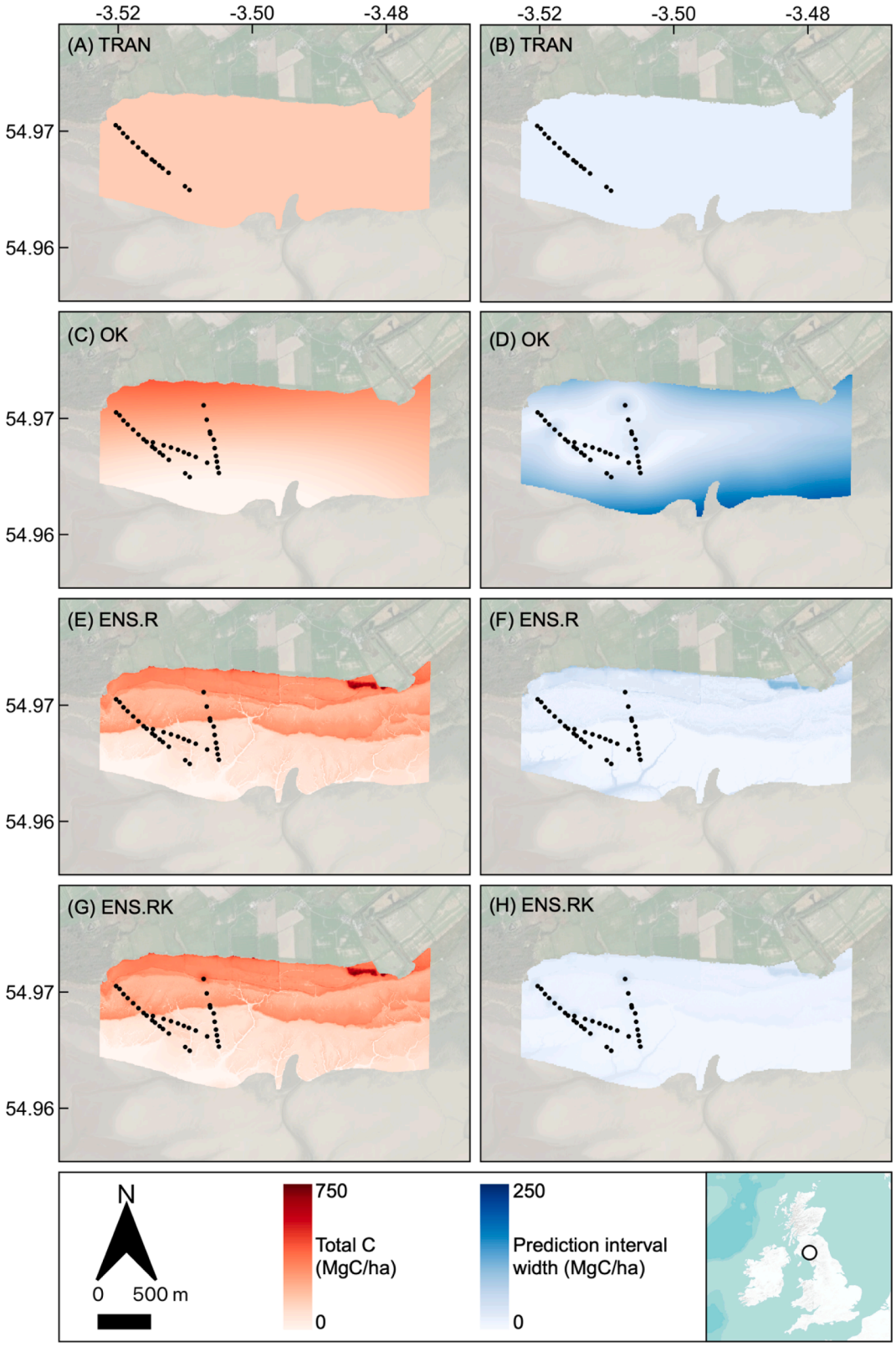

Fig. 6. Stock (red) and uncertainty (blue) of SOC upscaled from full soil cores for a section of Caerlaverock salt marsh, Scotland. Each map was generated from the best performing technique for each upscaling class (see Table 2). The specific upscaling technique is reported in each map panel. Uncertainty is presented using the 90% prediction interval width calculated from a leave-one-out cross validation resampling procedure, where high values indicate greater uncertainty. Elevation was used as the predictor in the regression models. Black dots indicate the location soil cores were gathered. (For interpretation of the references to colour in this figure legend, the reader is referred to the web version of this article.)

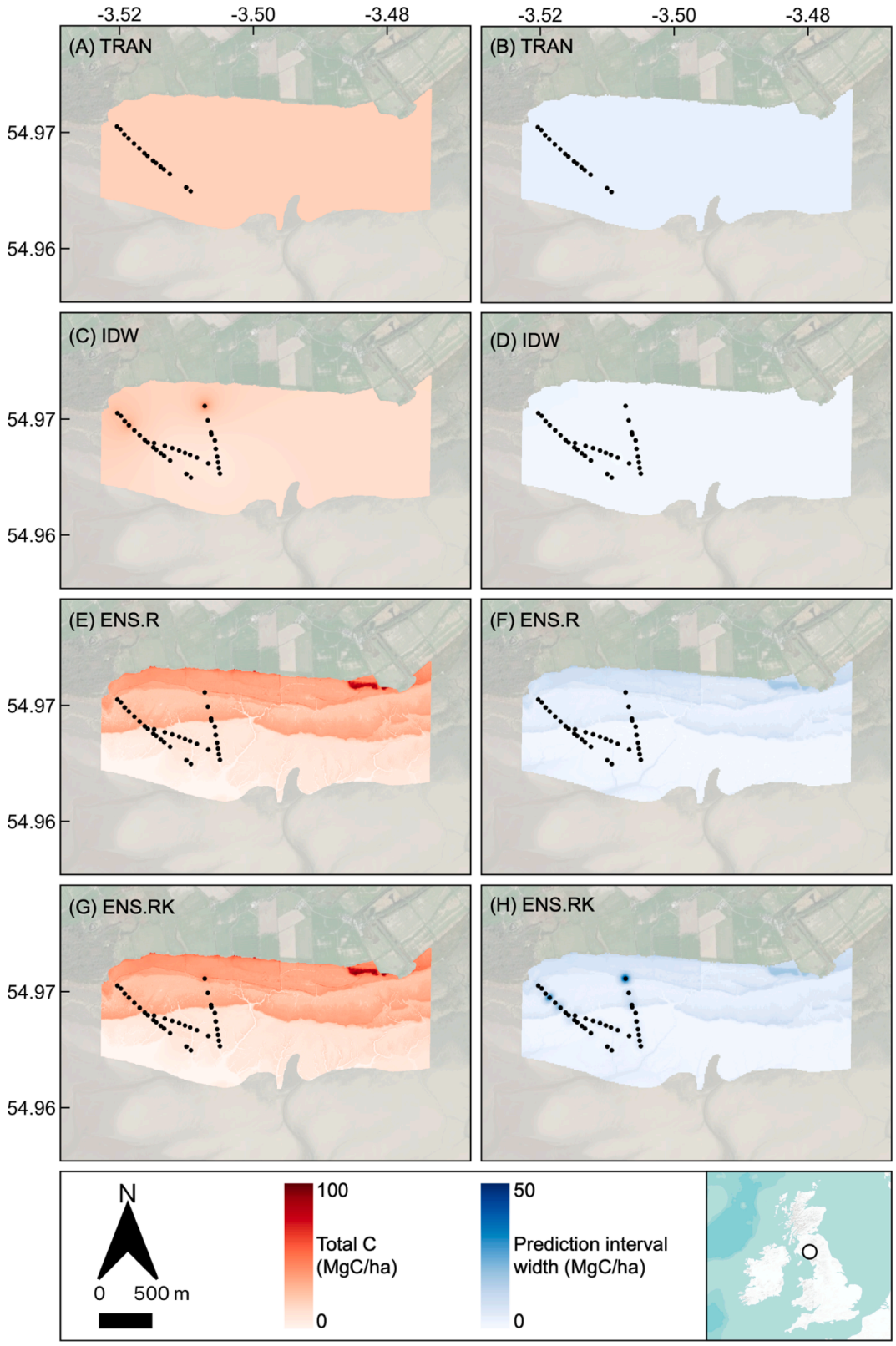

Fig. 7. Stock (red) and uncertainty (blue) of SOC upscaled from stratified soil cores for a section of Caerlaverock salt marsh, Scotland. Each map was generated from the best performing technique for each upscaling class (see Table 2). The specific upscaling technique is reported in each map panel. Uncertainty is presented using the 90% prediction interval width calculated from a leave-one-out cross validation resampling procedure, where high values indicate greater uncertainty. Elevation was used as the predictor in the regression models. Black dots indicate the location soil cores were gathered. (For interpretation of the references to colour in this figure legend, the reader is referred to the web version of this article.)

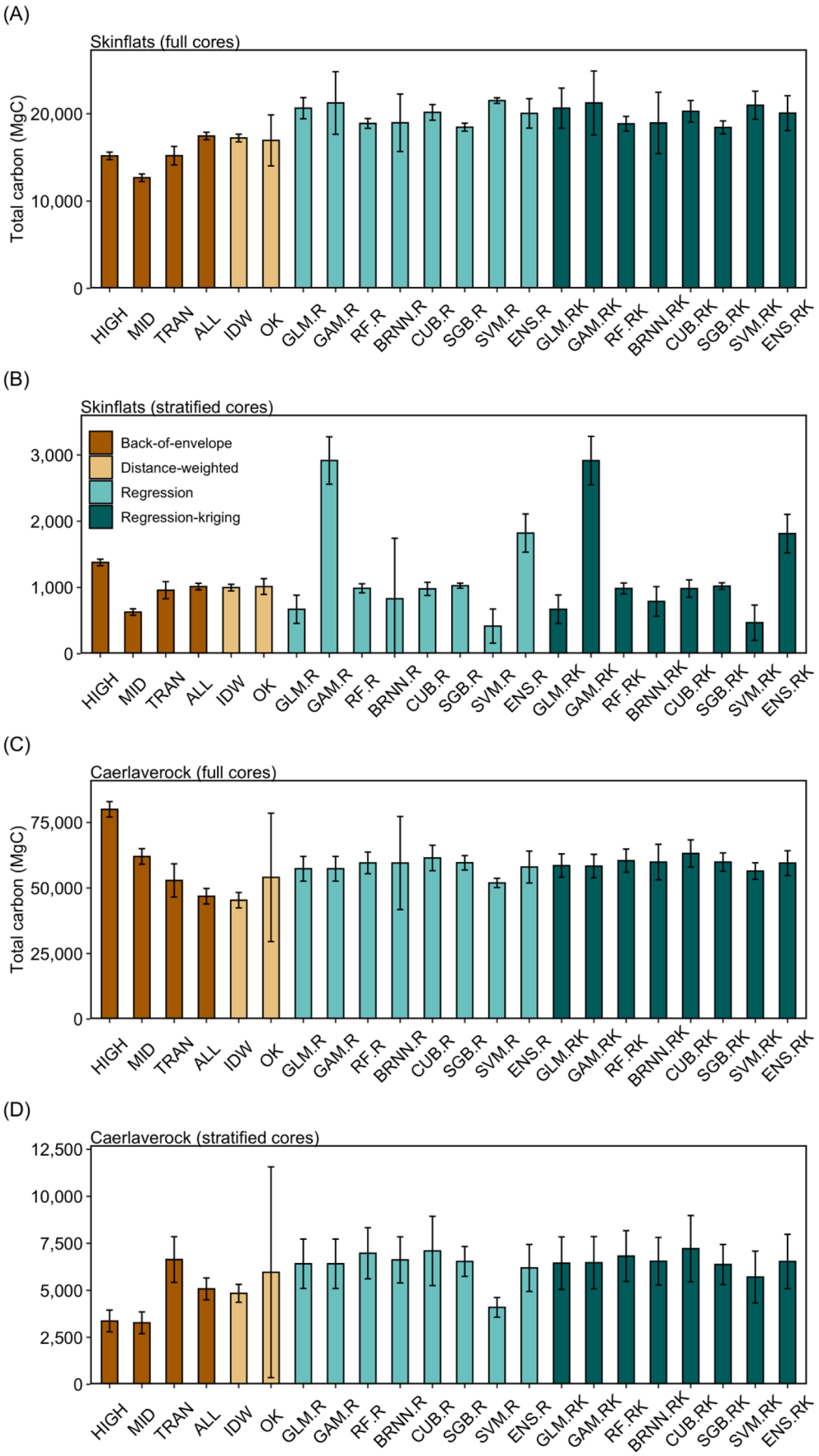

Fig. 8. Marsh-scale SOC content calculated from 22 upscaling techniques for Skinflats (**A** full and **B** stratified soil cores) and Caerlaverock (**C** full and **D** stratified soil cores). Error bars represent the 90% prediction interval width calculated from a leave-one-out cross validation resampling procedure.

policy briefings that argue for conservation and restoration measures (e.g., Spalding et al., 2021). Overstating the blue carbon value of an ecosystem would jeopardise SOC stock assessments upon which policy and planning is being increasingly based (Gulliver et al., 2020). SOC values could also be understated if marsh deposits exceed 1 m. Whilst soil depths of pioneer plant zones can be negligible, mature deposits nearest the land can reach tens of metres deep (Allen, 2000). In addition to reporting SOC values for 1 m deposits (Howard et al., 2014; Kennedy et al., 2014), we advocate for the parallel reporting of soil SOC stocks for distinct ecosystem deposits, where these can be clearly identified within stratigraphic sequences.

Considering which upscaling technique to recommend, the ensemble of regression-based models consistently performed the best in our uncertainty tests (after checking the strength of SOC-predictor correlations, evidence of bias in observed-predicted SOC values, and prediction interval width ranges in SOC distribution maps). We therefore consider ensemble upscaling to be the closest estimate of the true SOC content of salt marshes in our study. This finding has several important implications. Firstly, satellite derived DTM and NDVI surfaces are now freely available for much of the globe (such as the Sentinel (Pham et al., 2019a) and Shuttle Radar Topography Missions (Zhao et al., 2018)), offering the possibility of generating global and accurate marsh SOC stock calculations (Holmquist et al., 2018; Pham et al., 2019b) in combination with ensemble machine learning. Secondly, regression models produce detailed maps that show how SOC is distributed throughout marsh soils, unlike back-of-envelope calculations which assume a homogeneous SOC distribution, or distance-weighted calculations which fail to account for sharp transitions in topography or plant community common in salt marshes (e.g., the presence of marsh terraces in Caerlaverock). Detailed SOC maps can help managers identify valuable and vulnerable parts of a marsh for targeted and cost-effective intervention at metre scales, and any unrealistic values can be easily identified using associated error surfaces. For example, the maps for Caerlaverock also clearly demonstrate that soils with the highest SOC content are located nearest the land, in agreement with other studies (van Ardenne et al., 2018). The key driver of marsh loss across Great Britain has been the reclamation of landward facing marsh margins (Ladd, 2021), which causes the disproportionate loss of carbon dense marshland. Detailed SOC maps can therefore demonstrate how much SOC would be lost from human intervention. Thirdly, we found that a sample size as low as 26 soil cores was sufficient to produce accurate models of SOC stock calculation, in combination with well-fitted regression models; well below the recommended minimum sample size of 40 (Young et al., 2018). Moreover, back-of-envelope calculations that used multiple cores generally resulted in ballpark figures comparable to ensemble models. SOC values calculated from representative sampling, or shore-normal transects taken along the marsh, offer a suitably accurate alternative where covariate surfaces are unavailable for regression-based upscaling methods. In contrast, upscaling from single cores produced values that, at worse, varied by 65 % from ensemble calculations. We therefore caution against upscaling from single cores alone, to avoid over- or underestimating marsh-scale SOC stocks.

Ensemble regression models performed well, despite the poor correlation between DTM and NDVI at Skinflats. A weak correlation between DTM and NDVI on SOC stock could be the result of the relatively homogeneous topography and low floristic diversity of the marsh (Haynes, 2016). DTM values ranged by only 0.4 m compared to 5 m in Caerlaverock, and NDVI values similarly had a restricted range of 0.08 (see Appendix A). Low variation in DTM and NDVI values could amplify errors introduced in the generation the covariate surfaces, resulting in a weaker correlation with soil SOC content. The use of alternative covariate predictor surfaces could improve regression model fits. For example, Gholizadeh et al. (2018) used 18 different satellite band indices to predict SOC in agricultural sites. Marsh morphology, floristic composition, and microclimate will likely vary from site to site (Gorham et al., 2021), therefore optimum covariates are likely to be marsh-specific (Guevara et al., 2018). Nevertheless, accurate SOC stock calculations can still be achieved when taking the weighted average of multiple regression models even when built on poorly correlated covariates.

Interpolations perform poorly beyond where point samples are taken for distance-weighted classes and, by extension, regression-kriging techniques (Hengl and MacMillan, 2019). The performance of distance-weighted models can be improved if a gridded sampling design is adopted across the entire target site, with additional sampling taken along sharp topographic and vegetation community boundaries (van Ardenne et al., 2018). Regression models are less susceptible to under-representative sampling, since SOC stocks can be calculated across a range of DTM and NDVI values. However, any bias in the regression model can over- or under-estimate SOC stocks. Bias can be detected using observed-predicted plots (Bennett et al., 2013) and some bias was evident in all regression models nearest the tail ends of predicted SOC stocks. Prediction interval width surfaces again provide a means to detect where bias may exist in soil maps, here most notably along channels and marsh edges. Prediction interval width surfaces therefore provide a helpful tool for managers to identify areas where additional soil SOC sampling could improve marsh-scale SOC stock calculations.

There is a growing need to better quantify the world's carbon stores, to better measure progress towards mitigating climate change (e.g., for the '4 per 1000′ initiative; Minasny et al., 2017). Upscaling techniques described here apply to any scenario where large-scale SOC calculations can be derived from point samples and (where applicable) covariate surfaces. Our findings are therefore useful in calculating the carbon content of other terrestrial and marine deposits.

6. Conclusion

Policymakers require accurate inventories of soil SOC stock to inform conservation management, and therefore use of an appropriate sampling strategy and upscaling method are needed. Ensemble regression models from the weighted average of seven machine-learning algorithm calculations yielded the highest accuracy, even when covariate surfaces correlated poorly. Regression-based models have the advantage of producing detailed soil SOC and associated uncertainty maps, which can be used to identify SOC hotspots, anomalous values, and data-sparse regions. Covariate surfaces of key SOC predictors, such as elevation and vegetation composition, are now globally available and offer the possibility of generating large-scale and detailed soil SOC maps in salt marshes and other coastal vegetated systems. Simpler average values or distance-weighted techniques of a well-sampled marsh offer comparable marsh-scale SOC estimates to regression-based models; however, prediction surfaces poorly represent the distribution of SOC throughout the marsh. The use of single measures to upscale SOC stock should be avoided, as single values may poorly represent the entire marsh and can bias total SOC stocks. Average SOC values of multiple cores taken either along single or multiple transects produce marsh-scale SOC stocks equivalent to 'state-of-the-art' machine learning tools and are especially appropriate if no covariate surfaces of the target site are available. We also advocate for the dual reporting of SOC stocks calculated from both the standard 1 m sampling depth and for the full depth of modern marsh deposits, for a fairer representation of the actual blue carbon value per site. Our findings also apply to non-coastal environments, where determining the SOC stock of a region from point measures is required.

Declaration of Competing Interest

The authors declare that they have no known competing financial interests or personal relationships that could have appeared to influence the work reported in this paper.

Data availability

The soil core data used this study is held in the Environmental Information Data Centre repository, available at: https://catalogue.ceh.ac.uk/documents/5cc9ee72-ed88-4e71-bd8d-e3511bb9ed12.

Acknowledgements

This work was supported by the Natural Environment Research Council (grant NE/R010846/1) Carbon Storage in Intertidal Environments (C-SIDE) project. We thank Lucy Miller, Simone Riegel, and Levi Austin for their valuable contribution to the fieldwork campaigns.

Appendix A. Supplementary data

Supplementary data to this article can be found online at https://doi.org/10.1016/j.geoderma.2022.116188.

References

Allen, J.R.L., 1989. Evolution of salt-marsh cliffs in muddy and sandy systems: a qualitative comparison of British West-Coast estuaries. Earth Surf. Process. Landf. 14 (1), 85–92. https://doi.org/10.1002/esp.3290140108.

Allen, J.R.L., 2000. Morphodynamics of Holocene salt marshes: a review sketch from the Atlantic and Southern North Sea coasts of Europe. Quat. Sci. Rev. 19 (12), 1155–1231. https://doi.org/10.1016/S0277-3791(99)00034-7.

Atwood, T.B., Connolly, R.M., Almahasheer, H., Carnell, P.E., Duarte, C.M., Ewers Lewis, C.J., Irigoien, X., Kelleway, J.J., Lavery, P.S., Macreadie, P.I., Serrano, O., Sanders, C.J., Santos, I., Steven, A.D.L., Lovelock, C.E., 2017. Global patterns in mangrove soil carbon stocks and losses. Nat. Clim. Change 7, 523–528. https://doi.org/10.1038/nclimate3326.

Bai, J., Zhang, G., Zhao, Q., Lu, Q., Jia, J., Cui, B., Liu, X., 2016. Depth-distribution patterns and control of soil organic carbon in coastal salt marshes with different plant covers. Sci. Rep. 6, 34835. https://doi.org/10.1038/srep34835.

Beaumont, N.J., Jones, L., Garbutt, A., Hansom, J.D., Toberman, M., 2014. The value of carbon sequestration and storage in coastal habitats. Estuar. Coast. Shelf Sci. 137, 32–40. https://doi.org/10.1016/j.ecss.2013.11.022.

Bennett, N.D., Croke, B.F.W., Guariso, G., Guillaume, J.H.A., Hamilton, S.H., Jakeman, A.J., Marsili-Libelli, S., Newham, L.T.H., Norton, J.P., Perrin, C., Pierce, S. A., Robson, B., Seppelt, R., Voinov, A.A., Fath, B.D., Andreassian, V., 2013. Characterising performance of environmental models. Environ. Model. Softw. 40, 1–20. https://doi.org/10.1016/j.envsoft.2012.09.011.

Bishop, T.F.A., McBratney, A.B., Laslett, G.M., 1999. Modelling soil attribute depth functions with equal-area quadratic smoothing splines. Geoderma 91 (1–2), 27–45. https://doi.org/10.1016/S0016-7061(99)00003-8.

Copernicus Open Access Hub, 2021. (accessed 6 April 2022).

Crosby, S.C., Sax, D.F., Palmer, M.E., Booth, H.S., Deegan, L.A., Bertness, M.D., Leslie, H. M., 2016. Salt marsh persistence is threatened by predicted sea-level rise. Estuar. Coast. Shelf Sci. 181, 93–99. https://doi.org/10.1016/j.ecss.2016.08.018.

Duarte, C.M., Losada, I.J., Hendriks, I.E., Mazarrasa, I., Marbà, N., 2013. The role of coastal plant communities for climate change mitigation and adaptation. Nat. Clim. Change 3, 961–968. https://doi.org/10.1038/nclimate1970.

EDINA Digimap, 2019. https://digimap.edina.ac.uk (accessed 6 April 2022).

Ford, H., Garbutt, A., Duggan-Edwards, M., Pagés, J.F., Harvey, R., Ladd, C., Skov, M.W., 2019. Large-scale predictions of salt-marsh carbon stock based on simple observations of plant community and soil type. Biogeosciences 16, 425–436. https://doi.org/10.5194/bg-16-425-2019.

Gholizadeh, A., Žižala, D., Saberioon, M., Borůvka, L., 2018. Soil organic carbon and texture retrieving and mapping using proximal, airborne and Sentinel-2 spectral imaging. Remote Sens. Environ. 218, 89–103. https://doi.org/10.1016/j.rse.2018.09.015.

Gorham, C., Lavery, P., Kelleway, J., Salinas, C., Serrano, O., 2021. Soil carbon stocks vary across geomorphic settings in Australian temperate tidal marsh ecosystems. Ecosystems 24, 319–334. https://doi.org/10.1007/s10021-020-00520-9.

Guevara, M., Olmedo, G.F., Stell, E., Yigini, Y., Aguilar Duarte, Y., Arellano Hernández, C., Arévalo, G.E., Arroyo-Cruz, C.E., Bolivar, A., Bunning, S., Bustamante Cañas, N., Cruz-Gaistardo, C.O., Davila, F., Dell Acqua, M., Encina, A., Figueredo Tacona, H., Fontes, F., Hernández Herrera, J.A., Ibelles Navarro, A.R., Loayza, V., Manueles, A.M., Mendoza Jara, F., Olivera, C., Osorio Hermosilla, R., Pereira, G., Prieto, P., Ramos, I.A., Rey Brina, J.C., Rivera, R., Rodríguez-Rodríguez, J., Roopnarine, R., Rosales Ibarra, A., Rosales Riveiro, K.A., Schulz, G.A., Spence, A., Vasques, G.M., Vargas, R.R., Vargas, R., 2018. No silver bullet for digital soil mapping: country-specific soil organic carbon estimates across Latin America. SOIL 4 (3), 173–193. https://doi.org/10.5194/soil-4-173-2018.

Gulliver, A., Carnell, P.E., Trevathan-Tackett, S.M., de Paula, D., Costa, M., Masqué, P., Macreadie, P.I., 2020. Estimating the potential blue carbon gains from tidal marsh rehabilitation: a case study from South Eastern Australia. Front. Mar. Sci. 7, 403. https://doi.org/10.3389/fmars.2020.00403.

Hamilton, C.A., Lloyd, J.M., Barlow, N.L.M., Innes, J.B., Flecker, R., Thomas, C.P., 2017. Late Glacial to Holocene relative sea-level change in Assynt, northwest Scotland. UK. Quat. Res. 84, 214–222. https://doi.org/10.1016//j.yqres.2015.07.001.

Harris, D., Horwáth, W.R., van Kessel, C., 2001. Acid fumigation of soils to remove carbonates prior to total organic carbon or CARBON-13 isotopic analysis. Soil Sci. Soc. Am. J. 65 (6), 1853–1856. https://doi.org/10.2136/sssaj2001.1853.

Haynes, T.A., 2016. Scottish saltmarsh survey national report (Number 786). Scottish Natural Heritage, Inverness https://www.nature.scot/doc/naturescot-commissioned-report-786-scottish-saltmarsh-survey-national-report.

Hengl, T., MacMillan, R.A., 2019. Predictive soil mapping with R. OpenGeoHub foundation, Wageningen. https://soilmapper.org.

Herbert, E.R., Windham-Myers, L., Kirwan, M.L., 2021. Sea-level rise enhances carbon accumulation in United States tidal wetlands. One Earth 4 (3), 425–433. https://doi.org/10.1016/j.oneear.2021.02.011.

Hiemstra, P., 2013. Package 'automap' (Version 1.0-16). CRAN. https://cran.r-project.org/web/packages/automap/automap.pdf.

Hilmi, N., Chami, R., Sutherland, M.D., Hall-Spencer, J.M., Lebleu, L., Benitez, M.B., Levin, L.A., 2021. The role of blue carbon in climate change mitigation and carbon stock conservation. Front. Clim. 3, 710546 https://doi.org/10.3389/fclim.2021.710546.

Hinson, A.L., Feagin, R.A., Eriksson, M., Najjar, R.G., Herrmann, M., Bianchi, T.S., Kemp, M., Hutchings, J.A., Crooks, S., Boutton, T., 2017. The spatial distribution of soil organic carbon in tidal wetland soils of the continental United States. Glob. Chang. Biol. 23 (12), 5468–5480. https://doi.org/10.1111/gcb.13811.

Holmquist, J.R., Windham-Myers, L., Bliss, N., Crooks, S., Morris, J.T., Megonigal, J.P., Troxler, T., Weller, D., Callaway, J., Drexler, J., Ferner, M.C., Gonneea, M.E., Kroeger, K.D., Schile-Beers, L., Woo, I., Buffington, K., Breithaupt, J., Boyd, B.M., Brown, L.N., Dix, N., Hice, L., Horton, B.P., MacDonald, G.M., Moyer, R.P., Reay, W., Shaw, T., Smith, E., Smoak, J.M., Sommerfield, C., Thorne, K., Velinsky, D., Watson, E., Grimes, K.W., Woodrey, M., 2018. Accuracy and precision of tidal wetland soil carbon mapping in the conterminous United States. Sci. Rep. 8, 9478. https://doi.org/10.1038/s41598-018-26948-7.

Horton, B.P., Shennan, I., Bradley, S.L., Cahill, N., Kirwan, M., Kopp, R.E., Shaw, T.A., 2018. Predicting marsh vulnerability to sea-level rise using Holocene relative sea-level data. Nat. Commun. 9, 2687. https://doi.org/10.1038/s41467-018-05080-0.

Howard, J., Hoyt, S., Isensee, K., Telszewski, M., Pidgeon, E., 2014. Coastal blue carbon: methods for assessing carbon stocks and emissions factors in mangroves, tidal salt marshes, and seagrasses. International Union for Conservation of Nature, Gland https://www.cifor.org/knowledge/publication/5095/.

Jenny, H., 1994. Factors of soil formation: a system of quantitative pedology. Dover Publications Inc., New York.

Kelleway, J.J., Saintilan, N., Macreadie, P.I., Ralph, P.J., 2016. Sedimentary factors are key predictors of carbon storage in SE Australian saltmarshes. Ecosystems 19, 865–880. https://doi.org/10.1007/s10021-016-9972-3.

Kelleway, J.J., Saintilan, N., Macreadie, P.I., Baldock, J.A., Ralph, P.J., 2017. Sediment and carbon deposition vary among vegetation assemblages in a coastal salt marsh. Biogeosciences 14 (16), 3763–3779. https://doi.org/10.5194/bg-14-3763-2017.

Kempen, B., Dalsgaard, S., Kaaya, A.K., Chamuya, N., Ruipérez-González, M., Pekkarinen, A., Walsh, M.G., 2019. Mapping topsoil organic carbon concentrations and stocks for Tanzania. Geoderma 337, 164–180. https://doi.org/10.1016/j.geoderma.2018.09.011.

Kennedy, H., Alongi, D.M., Karim, A., Chen, G., Chmura, G.L., Crooks, S., Kairo, J.G., Liao, B., Lin, G., Troxler, T.G., 2013. Chapter 4: coastal wetlands. In: Hiraishi, T., Krug, T., Tanabe, K., Srivastava, N., Baasansuren, J., Fukuda, M., Troxler, T.G. (Eds.), 2013 Supplement to the 2006 IPCC Guidelines for National Greenhouse Gas Inventories: Wetlands. IPCC, Hayama, pp. 154–208 https://www.ipcc.ch/site/assets/uploads/2018/03/Wetlands_Supplement_Entire_Report.pdf.

Knotters, M., Brus, D.J., Voshaar, J.O., 1995. A comparison of kriging, co-kriging and kriging combined with regression for spatial interpolation of horizon depth with censored observations. Geoderma 67 (3–4), 227–246. https://doi.org/10.1016/0016-7061(95)00011-C.

Kuhn, M., 2008. Building predictive models in R using the caret package. J. Stat. Softw. 28 (5), 1–26. https://doi.org/10.18637/jss.v028.i05.

Ladd, C.J.T., 2021. Review on processes and management of saltmarshes across Great Britain. Proc. Geol. Assoc. 132 (3), 269–283. https://doi.org/10.1016/j.pgeola.2021.02.005.

LandIS, 2020. http://www.landis.org.uk (accessed 6 April 2022).

Li, J., Heap, A.D., Potter, A., Daniell, J.J., 2011. Application of machine learning methods to spatial interpolation of environmental variables. Environ. Model. Softw. 26 (12), 1647–1659. https://doi.org/10.1016/j.envsoft.2011.07.004.

Li, J., Heap, A.D., 2011. A review of comparative studies of spatial interpolation methods in environmental sciences: performance and impact factors. Ecol. Inform. 6 (3–4), 228–241. https://doi.org/10.1016/j.ecoinf.2010.12.003.

Ließ, M., Schmidt, J., Glaser, B., 2016. Improving the spatial prediction of soil organic carbon stocks in a complex tropical mountain landscape by methodological specifications in machine learning approaches. PLoS ONE 11, e0153673. 10.1371/journal.pone.0153673.

Luisetti, T., Turner, R.K., Andrews, J.E., Jickells, T.D., Kröger, S., Diesing, M., Paltriguera, L., Johnson, M.T., Parker, E.R., Bakker, D.C.E., Weston, K., 2019. Quantifying and valuing carbon flows and stores in coastal and shelf ecosystems in the UK. Ecosyst. Serv. 35, 67–76. 10.1016/j.ecoser.2018.10.013.

MacDonald, M.A., de Ruyck, C., Field, R.H., Bedford, A., Bradbury, R.B., 2017. Benefits of coastal managed realignment for society: evidence from ecosystem service assessments in two UK regions. Estuar. Coast. Shelf Sci. 244, 105609. 10.1016/j.ecss.2017.09.007.

Macreadie, P.I., Nielsen, D.A., Kelleway, J.J., Atwood, T.B., Seymour, J.R., Petrou, K., Connolly, R.M., Thomson, A.C., Trevathan-Tackett, S.M., Ralph, P.J., 2017a. Can we manage coastal ecosystems to sequester more blue carbon? Front. Ecol. Environ. 15, 206–213. https://doi.org/10.1002/fee.1484.

Macreadie, P.I., Ollivier, Q.R., Kelleway, J.J., Serrano, O., Carnell, P.E., Ewers Lewis, C. J., Atwood, T.B., Sanderman, J., Baldock, J., Connolly, R.M., Duarte, C.M., Lavery, P. S., Steven, A., Lovelock, C.E., 2017b. Carbon sequestration by Australian tidal marshes. Sci. Rep. 7, 44071. https://doi.org/10.1038/srep44071.

Macreadie, P.I., Anton, A., Raven, J.A., Beaumont, N., Connolly, R.M., Friess, D.A., Kelleway, J.J., Kennedy, H., Kuwae, T., Lavery, P.S., Lovelock, C.E., Smale, D.A., Apostolaki, E.T., Atwood, T.B., Baldock, J., Bianchi, T.S., Chmura, G.L., Eyre, B.D., Fourqurean, J.W., Hall-Spencer, J.M., Huxham, M., Hendriks, I.E., Krause-Jensen, D., Laffoley, D., Luisetti, T., Marbà, N., Masque, P., McGlathery, K.J., Megonigal, J.P., Murdiyarso, D., Russell, B.D., Santos, R., Serrano, O., Silliman, B.R., Watanabe, K., Duarte, C.M., 2019. The future of Blue Carbon science. Nat. Commun. 10, 3998. https://doi.org/10.1038/s41467-019-11693-w.

Marshall, J.R., 1962. The morphology of the upper Solway salt marshes. Scottish Geogr. Mag. 78 (2), 81–99. https://doi.org/10.1080/00369226208735859.

Mayer, B., Kylling, A., 2005. Technical note: the libRadtran software package for radiative transfer calculations - description and examples of use. Atmos. Chem. Phys. 5 (7), 1855–1877. https://doi.org/10.5194/acp-5-1855-2005.

Mcleod, E., Chmura, G.L., Bouillon, S., Salm, R., Björk, M., Duarte, C.M., Lovelock, C.E., Schlesinger, W.H., Silliman, B.R., 2011. A blueprint for blue carbon: toward an improved understanding of the role of vegetated coastal habitats in sequestering CO_2. Front. Ecol. Environ. 9 (19), 552–560. https://doi.org/10.1890/110004.

Minasny, B., Malone, B.P., McBratney, A.B., Angers, D.A., Arrouays, D., Chambers, A., Chaplot, V., Chen, Z.-S., Cheng, K., Das, B.S., Field, D.J., Gimona, A., Hedley, C.B., Hong, S.Y., Mandal, B., Marchant, B.P., Martin, M., McConkey, B.G., Mulder, V.L., O'Rourke, S., Richer-de-Forges, A.C., Odeh, I., Padarian, J., Paustian, K., Pan, G., Poggio, L., Savin, I., Stolbovoy, V., Stockmann, U., Sulaeman, Y., Tsui, C.-C., Vågen, T.-G., van Wesemael, B., Winowiecki, L., 2017. Soil carbon 4 per mille. Geoderma 292, 59–86.

Nieuwenhuize, J., Maas, Y.E., Middelburg, J.J., 1994. Rapid analysis of organic carbon and nitrogen in particulate materials. Mar. Chem. 45 (3), 217–224. https://doi.org/10.1016/0304-4203(94)90005-1.

Olaya-Abril, A., Parras-Alcántara, L., Lozano-García, B., Obregón-Romero, R., 2017. Soil organic carbon distribution in Mediterranean areas under a climate change scenario via multiple linear regression analysis. Sci. Total Environ. 592, 134–143. https://doi.org/10.1016/j.scitotenv.2017.03.021.

Owusu, S., Yigini, Y., Olmedo, G.F., Omuto, C.T., 2020. Spatial prediction of soil organic carbon stocks in Ghana using legacy data. Geoderma 360, 114008. https://doi.org/10.1016/j.geoderma.2019.114008.

Pebesma, E.J., 2004. Multivariable geostatistics in S: the gstat package. Comput. Geosci. 30 (7), 683–691. https://doi.org/10.1016/j.cageo.2004.03.012.

Pham, T.D., Xia, J., Baier, G., Le, N., Yokoya, N., 2019a. Mangrove species mapping using Sentinel-1 and Sentinel-2 data in North Vietnam. In: 2019 International Geoscience and Remote Sensing Symposium, pp. 6102–6105. https://doi.org/10.1109/IGARSS.2019.8898987.

Pham, T.D., Xia, J., Ha, N.T., Bui, D.T., Le, N.N., Tekeuchi, W., 2019b. A review of remote sensing approaches for monitoring Blue Carbon ecosystems: mangroves, seagrasses and salt marshes during 2010–2018. Sensors 19 (8), 1933. https://doi.org/10.3390/s19081933.

Rogers, K., Kelleway, J.J., Saintilan, N., Megonigal, J.P., Adams, J.B., Holmquist, J.R., Lu, M., Schile-Beers, L., Zawadzki, A., Mazumder, D., Woodroffe, C.D., 2019. Wetland carbon storage controlled by millennial-scale variation in relative sea-level rise. Nature 567 (7746), 91–95.

Rogers, Macreadie, P.I., Kelleway, J.J., Saintilan, N., 2019b. Blue carbon in coastal landscapes: a spatial framework for assessment of stocks and additionality. Sustain. Sci. 14, 453–467. 10.1007/s11625-018-0575-0.

Saintilan, N., Kovalenko, K.E., Guntenspergen, G., Rogers, K., Lynch, J.C., et al., 2022. Constraints on the adjustment of tidal marshes to accelerating sea level rise. Science 377 (6605), 523–527. https://doi.org/10.1126/science.abo7872.

Schuerch, M., Spencer, T., Temmerman, S., Kirwan, M.L., Wolff, C., Lincke, D., McOwen, C.J., Pickering, M.D., Reef, R., Vafeidis, A.T., Hinkel, J., Nicholls, R.J., Brown, S., 2018. Future response of global coastal wetlands to sea-level rise. Nature 561, 231–234. https://doi.org/10.1038/s41586-018-0476-5.

Shi, Z., Lamb, H.F., 1991. Post-glacial sedimentary evolution of a microtidal estuary, Dyfi Estuary, west Wales. UK. Sediment. Geol. 73 (3–4), 227–246. https://doi.org/10.1016/0037-0738(91)90086-s.

Smeaton, C., Barlow, N.L., Austin, W.E., 2020. Coring and compaction: best practice in blue carbon stock and burial estimations. Geoderma 364, 114180. https://doi.org/10.1016/j.geoderma.2020.114180.

Smeaton, C., Burden, A., Ruranska, P., Ladd, C.J.T., Garbutt, A., Jones, L., McMahon, L., Miller, L.C., Skov, M.W., Austin, W.E.N., 2022. Using citizen science to estimate surficial soil blue carbon stock in Great British saltmarshes. Front. Mar. Sci. 9, 959459 https://doi.org/10.3389/fmars.2022.959459.

Smith, A.J., Kirwan, M.L., 2021. Sea level-driven marsh migration results in rapid net loss of carbon. Geophys. Res. Lett. 48 (13), e2021GL092420. 10.1029/2021GL092420.

Sousa, A.I., Santos, D.B., da Silva, E.F., Sousa, L.P., Cleary, D.F.R., Soares, A.M.V.M., Lillebø, A.I., 2017. 'Blue Carbon' and nutrient stocks of salt marshes at a temperate coastal lagoon (Ria de Aveiro, Portugal). Sci. Rep. 7, 41225. https://doi.org/10.1038/srep41225.

Spalding, M.D., Leal, M., 2021. The State of the world's mangroves 2021. Global Mangrove Alliance. https://www.mangrovealliance.org/wp-content/uploads/2021/07/The-State-of-the-Worlds-Mangroves-2021-FINAL.pdf.

Swindles, G.T., Galloway, J.M., Macumber, A.L., Croudace, I.W., Emery, A.R., Woulds, C., Bateman, M.D., Parry, L., Jones, J.M., Selby, K., Rushby, G.T., Baird, A. J., Woodroffe, S.A., Barlow, N.L.M., 2018. Sedimentary records of coastal storm surges: evidence of the 1953 North Sea event. Mar. Geol. 403, 262–270. https://doi.org/10.1016/j.margeo.2018.06.013.

Theuerkauf, E.J., Stephens, J.D., Ridge, J.T., Fodrie, F.J., Rodriguez, A.B., 2015. Carbon export from fringing saltmarsh shoreline erosion overwhelms carbon storage across a critical width threshold. Estuar. Coast. Shelf Sci. 164, 367–378. https://doi.org/10.1016/j.ecss.2015.08.001.

Thompson, B.S., Primavera, J.H., Friess, D.A., 2017. Governance and implementation challenges for mangrove forest Payments for Ecosystem Services (PES): empirical evidence from the Philippines. Ecosyst. Serv. 23, 146–155. https://doi.org/10.1016/j.ecoser.2016.12.007.

Tröels-Smith, J., 1955. Characterization of unconsolidated sediments, third vol. Danmarks Geologiske Undersogelse.

Ullman, R., Bilbao-Bastida, V., Grimsditch, G., 2013. Including Blue Carbon in climate market mechanisms. Ocean Coast. Manag. 83, 15–18. https://doi.org/10.1016/j.ocecoaman.2012.02.009.

van Ardenne, L.B., Jolicouer, S., Bérubé, D., Burdick, D., Chmura, G.L., 2018. The importance of geomorphic context for estimating the carbon stock of salt marshes. Geoderma 330, 264–275. https://doi.org/10.1016/j.geoderma.2018.06.003.

Van de Broek, M., Vandendriessche, C., Poppelmonde, D., Merckx, R., Temmerman, S., Govers, G., 2018. Long-term organic carbon sequestration in tidal marsh sediments is dominated by old-aged allochthonous inputs in a macrotidal estuary. Glob. Change Biol. 24, 2498–2512. https://doi.org/10.1111/gcb.14089.

Verardo, D.J., Froelich, P.N., McIntyre, A., 1990. Determination of organic carbon and nitrogen in marine sediments using the Carlo Erba NA-1500 analyzer. Deep Sea Res. Part A Oceanogr. Res. Pap. 37 (1), 157–165. https://doi.org/10.1016/0198-0149(90)90034-S.

Wang, F., Sanders, C.J., Santos, I.R., Tanh, J., Schuerch, M., et al., 2021. Global blue carbon accumulation in tidal wetlands increases with climate change. Natl. Sci. Rev. 8 (9), nwaa296. https://doi.org/10.1093/nsr/nwaa296.

Webb, A.J., Metcalfe, A.P., 1987. Physical aspects, water movements and modelling studies of the Forth estuary, Scotland. Proc. Royal Soc. Edinb. B Biol. Sci. 93, 259–272. https://doi.org/10.1017/S0269727000006722.

Young, M.A., Macreadie, P.I., Duncan, C., Carnell, P.E., Nicholson, E., Serrano, O., Duarte, C.M., Shiell, G., Baldock, J., Ierodiaconou, D., 2018. Optimal soil carbon sampling designs to achieve cost-effectiveness: a case study in blue carbon ecosystems. Biol. Lett. 14 (9), 20180416. https://doi.org/10.1098/rsbl.2018.0416.

Zhao, X., Su, Y., Hu, T., Chen, L., Gao, S., Wang, R., Jin, S., Guo, Q., 2018. A global corrected SRTM DEM product for vegetated areas. Remote Sens. Lett. 9 (4), 393–402. https://doi.org/10.1080/2150704X.2018.1425560.